

# Averaging methods for cavitating bubbly flows

S. H. Bryngelson,<sup>1</sup> A. Charalampopoulos,<sup>2</sup> T. P. Sapsis,<sup>2</sup> T. Colonius<sup>1</sup>

(California Institute of Technology<sup>1</sup>, Massachusetts Institute of Technology<sup>2</sup>, USA)

## ABSTRACT

Averaged models are used to represent cavitating bubbly mixtures at the sub-grid computational level. Though such averaging techniques are widely used, the relative computational performance of various adaptations remains unknown. The accuracy and computational efficiency of two such models, one ensemble-averaging and one volume-averaging, addresses this issue. Results show that the relative computational cost of the methods depends upon the degree of bubble polydispersity. The ensemble-averaged model requires more quadrature nodes for broader population sizes and increasingly broad populations become computationally untenable. A moment-based method addresses this shortcoming. It uses a Gaussian closure and is augmented via long short-term memory recurrent neural networks for high-order statistics. Results show that this approach achieves small relative errors for even high-order statistical moments using only five degrees of freedom, significantly fewer than the hundreds required by classes methods.

## INTRODUCTION

Cavitation bubbles oscillate, expand by several orders of magnitude in radius, and violently collapse. Flow features of cavitation bubble mixtures can be as sensitive to this bubble motion as they are to bulk-scale pressure waves (Reisman et al., 1998). Thus, faithful representations of the bubble-scale dynamics are central to the predictive capabilities of bubbly flow simulations. Numerous medical engineering applications motivate such simulation development. Bubbles nucleate during lithotripsy (Pishchalnikov et al., 2003) to ablate kidney stones, though they can also emerge near propellers (Sharma et al., 1990; Ji et al., 2012) or in hydraulic pipe systems (Weyler et al., 1971; Streeter, 1983), causing damage and noise. Large numbers of micron-scale bubbles often emerge in these engineering flows, while the bulk-flow features can be meter-scale or larger (Brennen, 1995). In such cases, resolving the bubble interfaces and their dynamics are prohibitive and must be modeled. Note that phenomena like sheet cavitation over propellers can involve micron-scale bubbles, larger-scale gas and vapor regions, and periods of transition between the

two. Faithful models for this do not yet exist and are not considered herein.

Averaging approaches are useful when the bubble interfaces cannot be resolved. They couple a Rayleigh–Plesset-like equation for the bubble dynamics to the motion of the continuous phase. Such models are either ensemble- (Zhang and Prosperetti, 1994) or volume-averaging (Biesheuvel and van Wijngaarden, 1984). We consider the relative computational cost and agreement between these methods. Of particular interest is the ability of the models to represent polydisperse bubble populations. Polydispersity has a significant impact of the flow, damping and dispersing averaged pressure fluctuations (Colonius et al., 2008). Representing these dynamics requires statistical-moments of the bubble population. A typical technique for computing these moments is the method of classes (Vanni, 2000). It discretizes the integrand into bins and evolves them. However, the number of bins must increase as the broadness of the population increases to maintain the same accuracy.

A moment method can address this issue; they represent the integrand via parameters of a probability density function. This approach can represent, for example, bubble coalescence and breakup (Heylman et al., 2019) and dilute gas-particle flows (Capecehatro and Desjardins, 2013). The model evolves a set of shape parameters for a Gaussian distribution. This evolution follows from a population balance equation and is closed via probability calculus. However, higher-order moments can develop during bubble cavitation. Representing these moments via more general density functions is expensive and often ill-posed. Instead, neural networks present a unique opportunity to augment the imperfect dynamical system via only simple training data based upon Monte Carlo predictions. In particular, long short-term memory (LSTM) recurrent neural networks (RNNs) are well-suited for this task. They can represent the time-dependent structure of bubble dynamics and have been used to improve or accelerate prediction of many fluid dynamics problems, including bubble advection (Wan et al., 2019) and near-wall turbulence (Srinivasan et al., 2019).

We first present the typical averaging models and their principal differences. The specific models we use follows, including their implementation in a numeri-

cal framework. The computational performance of these models is compared via a case study of an acoustically excited dilute bubble screen. Our new moment-based formulation is then presented. The method performance is evaluated for Rayleigh–Plesset bubbles under static pressure ratios. Future work will consider this model in a two-way coupled flow simulation environment.

## AVERAGED MODEL DESCRIPTIONS

Volume-averaging (Biesheuvel and van Wijngaarden, 1984) (figure 1 (a)) is a deterministic approach that represents bubbles as individual dynamic features; they are sampled from a distribution of equilibrium bubble radii and coupled to the liquid phase via local volume averaging and, in a computational setting, a volumetric smearing operator (Fuster and Colonius, 2011). Ensemble averaging (Zhang and Prosperetti, 1994) (figure 1 (b)) is instead a stochastic approach. This model uses bubble population moments to derive the governing mixture-averaged flow equations and bubble dynamics are evaluated on the Eulerian grid and advected via a transport equation. Both approaches represent polydispersity as a probability density function for the equilibrium bubble size. For the volume-averaged approach, knowledge of mean quantities requires an ensemble of simulations with different realizations of randomized bubble locations (and other properties), whereas the ensemble-averaged method bins and evolves the probability density function for the equilibrium bubble radius (Ando et al., 2011). The specific models we use assume that there is no relative motion between the bubbles and the carrier phase, that the bubbles are dilute, and that the gas density is much smaller than the liquid density.

## MODEL FORMULATION

The flow of a dilute suspension of evolving bubbles in a compressible liquid is cast in the quasi-conservative form

$$\frac{\partial \mathbf{q}}{\partial t} + \nabla \cdot \mathbf{F} = \mathbf{s} \quad (1)$$

where  $\mathbf{q} = \{\rho, \rho \mathbf{u}, E\}$  are the conservative variables,  $\mathbf{F} = \{\rho \mathbf{u}, \rho \mathbf{u} \mathbf{u} + p \mathbf{I}, (E + p) \mathbf{u}\}$  are the fluxes,  $\mathbf{s}$  are source terms, and  $\rho$ ,  $\mathbf{u}$ ,  $p$ , and  $E$  are the mixture density, velocity vector, pressure, and total energy, respectively. Governing equations (1) are solved using a fifth-order accurate finite-volume scheme with WENO reconstruction to compute spatial derivatives and the third-order accurate TVD Runge–Kutta algorithm for time integration.

The ensemble-averaged equations follows from Zhang and Prosperetti (1994) and Bryngelson et al. (2019). The polydisperse bubble population is log-normally distributed with shape parameter  $\sigma_p$  (Ando et al., 2011). A classes method with  $N_{\text{bin}}$  bins evolves its moments for the equilibrium bubble sizes  $\mathbf{R}_o$  as  $\mathbf{R}(\mathbf{R}_o) = \{R_1, R_2, \dots, R_{N_{\text{bin}}}\}$ . In this case  $\mathbf{s} = \mathbf{0}$  and the pressure is

$$p = (1 - \alpha)p_l + \alpha \left( \frac{\overline{\mathbf{R}^3 \mathbf{p}_b}}{\overline{\mathbf{R}^3}} - \rho \frac{\overline{\mathbf{R}^3 \dot{\mathbf{R}}^2}}{\overline{\mathbf{R}^3}} \right), \quad (2)$$

where  $\dot{\mathbf{R}}$  are the bubble radial velocities,  $\mathbf{p}_b$  are the bubble pressures, and the associated over-bars are statistical moments with respect to the  $R_o$  probability density function. The stiffened gas equation of state determines the liquid pressure  $p_l$ . A transport equation advects the void fraction as

$$\frac{\partial \alpha}{\partial t} + \mathbf{u} \cdot \nabla \alpha = 3\alpha \frac{\overline{\mathbf{R}^2 \dot{\mathbf{R}}}}{\overline{\mathbf{R}^3}}. \quad (3)$$

The volume averaging method follows Maeda and Colonius (2018):  $N_{\text{bub}}$  bubbles are located at Lagrangian points  $\mathbf{x}$  and evolve dynamically. The local

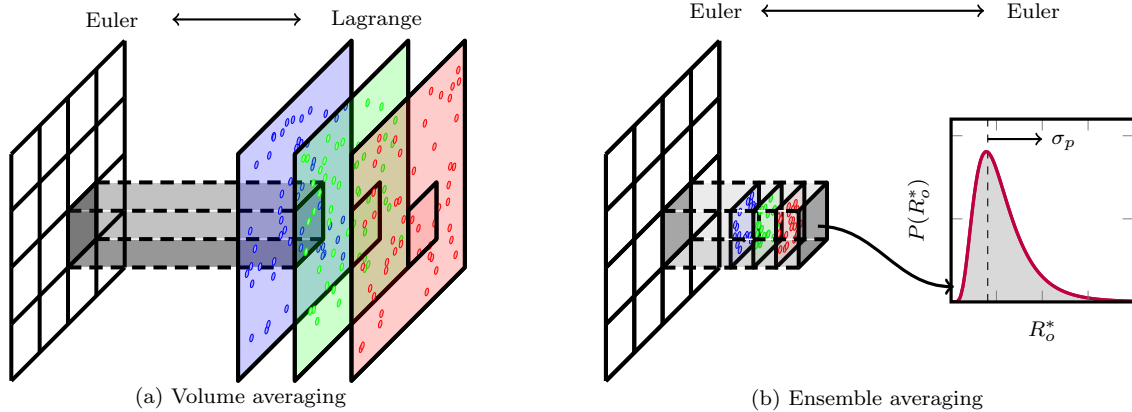


**Figure 1:** Schematic illustration of (a) volume- and (b) ensemble-averaged methods.

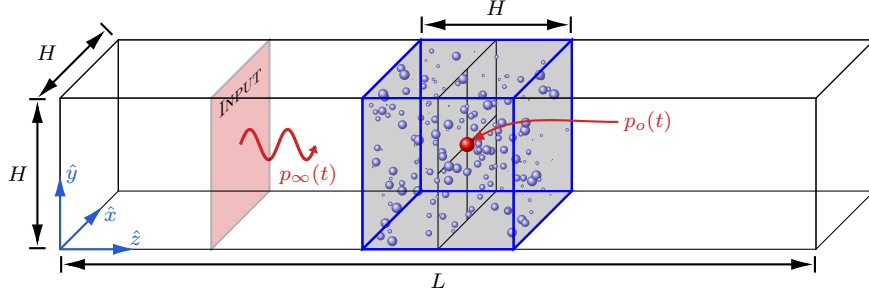


**Figure 2:** The model flow system.

void fraction field  $\alpha(\mathbf{x})$  is smeared onto the Eulerian grid via a Gaussian regularization kernel, modifying the void fraction advection equation (Maeda and Colonius, 2018). Thus, the source terms of (1) for the volume-averaged method are

$$\mathbf{s} = \frac{\mathbf{q}}{1 - \alpha} D_t \alpha, \quad (4)$$

where  $D_t$  is the substantial derivative operator, which transports the void fraction field.

The bubble dynamics in both cases are modeled as spherical gas regions that do not interact with each other. Their evolution is driven by the far-field pressure fluctuations  $p_\infty$  and modeled by the Keller–Miksis equation (Keller and Miksis, 1980). The resulting model dispersion can reproduce the sound speeds of actual bubbly mixtures (Ando, 2010).

## NUMERICAL METHODS

The governing equations (1) are solved with the multi-component flow code (MFC), an open-source compressible flow solver. An exposition of the solver is presented elsewhere (Bryngelson et al., 2019), so only a brief description is given here. Finite volumes discretize space and a 5th-order-accurate WENO scheme reconstructs the primitive variables at their faces (Coralic and Colonius, 2006). The HLLC approximate Riemann solver computes the associated fluxes (Toro et al., 1994) and a 3rd-order-accurate TVD Runge–Kutta scheme advances the solution in time (Gottlieb and Shu, 1998).

## MODEL COMPUTATIONAL PERFORMANCE AND COMPARISON

### Test problem setup and model equivalency

An acoustically excited dilute bubble screen serves as a case study for comparisons between the averaged methods (Bryngelson et al., 2019). A single cycle of a 300 kHz,  $p_A = 100$  kPa sinusoidal pressure pulse  $p_\infty(t)$  propagates towards a cubic bubble screen of initial void fraction  $\alpha_o$  and side-length  $H = L/5$ . The bubbles have

mean radius  $10 \mu\text{m}$ . The domain has length  $L = 25$  mm and characteristic-based boundary conditions suppress reflections at all domain boundaries. The quantity of interest is the pressure at the center of the bubble screen,  $p_o(t)$ .

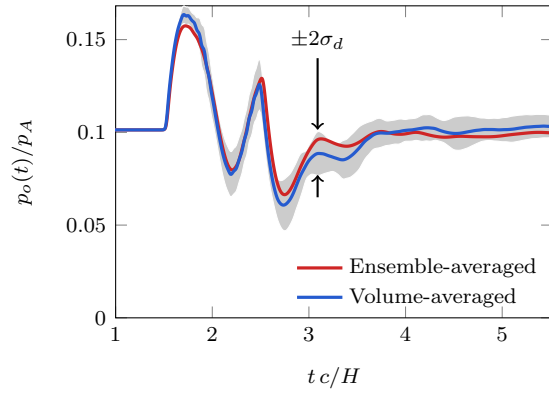


**Figure 3:** Evolution of the bubble-screen-centered pressure for both averaged techniques.  $\alpha_o = 4 \times 10^{-5}$  is the initial void fraction and  $\sigma_p = 0.3$  is the degree of polydispersity. The shaded region shows the  $\pm 2\sigma_d$  envelope of individual simulations, which  $\sigma_d$  is the standard deviation of those simulations. The mean volume-averaged curve is computed from 10 such simulations. Time is non-dimensionalized by the sound speed and the bubble screen side-length.

The first consideration is that the ensemble- and volume-averaged methods give the same result. Figure 3 shows the pressure at the center of the bubble screen for our test problem. The ensemble-averaged pressure matches the mean volume-averaged pressure to within two standard deviations of the individual simulations  $\sigma_d$ . Thus, the models converge to the same result to at least within this accuracy.

### Computational expense

The computational cost associated with the averaged models is an important consideration for large scale flow simulations. This cost depends upon the number of

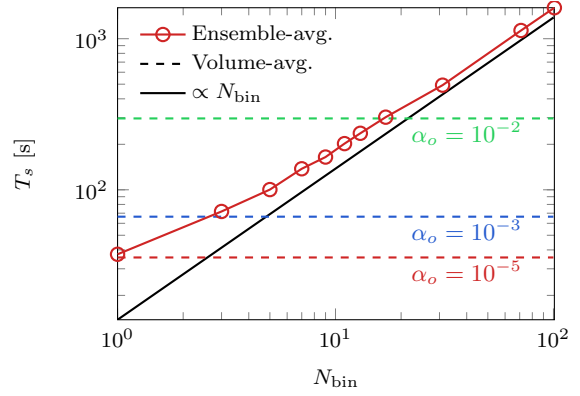
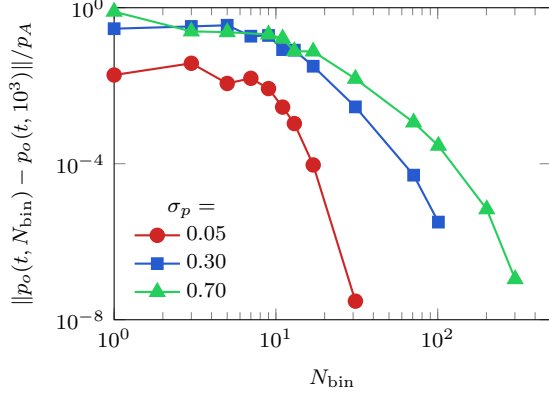


**Figure 4:** (Left) Convergence of ensemble-averaged simulations with  $N_{\text{bin}}$  for varying degrees of polydispersity  $\sigma_p$ . (Right) The time-step cost  $T_s$  in seconds for simulations of varying  $N_{\text{bin}}$  and  $\alpha_o$ , where  $N_{\text{bin}}$  is the number of bins used to approximate the log-normal bubble size density function.

bubbles (associated with  $\alpha_o$ ), the number of bins required to represent polydispersity  $N_{\text{bin}}$ , and the number of grid points associated with the simulation grid  $N$ . We first consider the expense associated with polydispersity, which can be significant because at least two bubble dynamics equations (depending upon the bubble model) append the flow equations for each bin.

Figure 4 (left) shows the error in the pressure at the center of the bubble screen when varying the number of bins used to discretize the probability density function. The error decreases exponentially, with larger errors observed for broader populations (larger  $\sigma_p$ ). For  $\sigma_p = 0.3$ ,  $N_{\text{bin}} = 11$  this error is 8% of  $p_A$  and for  $N_{\text{bin}} = 101$  the error is  $10^{-4}\%$ . Thus, broad populations require many bins (compared to the number of flow variables).

We next evaluate the averaged grind time per simulation time step  $T_s$ . Figure 4 (right) shows this  $T_s$  for varying bin numbers  $N_{\text{bin}}$ .  $T_s$  is independent of  $N_{\text{bin}}$  for the volume averaging cases because bins are not required from this method to represent polydispersity. Since increasing  $\alpha_o$  entails evolving more bubbles in the volume-averaged case,  $T_s$  increases with  $\alpha_o$ . For the ensemble averaged cases,  $T_s$  is approximately linear for  $N_{\text{bin}} \gtrsim 10$ . This is also the regime associated with most polydisperse simulations.

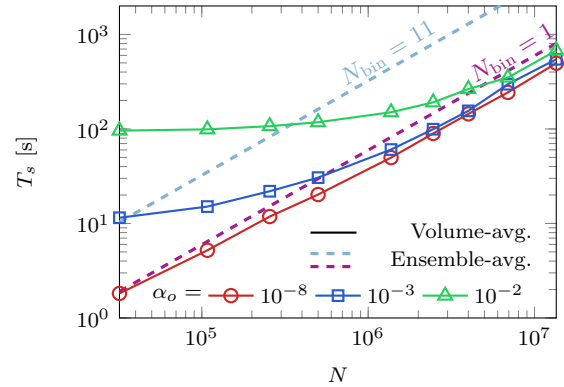


**Figure 5:** The time-step cost  $T_s$  in seconds for varying  $N$  and  $\alpha_o$ .

Figure 5 shows the  $T_s$  for different grid resolutions  $N$ . Ensemble-averaged cases are linear for all  $N$  because the bubble variables exist everywhere on the Eulerian mesh. For the volume-averaged cases  $T_s$  plateaus for small  $N$ . This is because evaluating the individual bubble dynamics exceeds the cost of evolving the Eulerian flow variables for such cases. Figure 5 also shows that for even a small  $N_{\text{bin}} = 11$  the ensemble-averaged simulations are more expensive than their volume-averaged counterparts for large  $N$  or small  $\alpha_o$ . Note that this does not account for the number of samples required for the volume-averaged cases to converge to a homogeneous mean flow (Bryngelson et al., 2019). The ensemble-averaged simulations are cheaper than the volume averaged cases for monodisperse populations ( $N_{\text{bin}} = 1$ ). Thus, we next focus on more efficient representations of polydisperse population dynamics.

## ACCELERATED MOMENT COMPUTATION

### Moment-based method formulation

The polydisperse bubble dynamics of section entails three uncertain variables:  $R$ ,  $\dot{R}$ , and  $R_o$ . We consider  $R_o$ -monodisperse cases to simplify our model formulation, though extending this is straightforward. The probability of any such state  $\vec{\mathbf{x}} = \{R, \dot{R}\}$  is

$$P = P(\vec{\mathbf{x}}, \vec{\boldsymbol{\theta}}, t), \quad (5)$$

where  $P$  is a bivariate probability density function with parameters (e.g. means, shape parameters)  $\vec{\boldsymbol{\theta}}$  and moments  $\vec{\boldsymbol{\mu}}'$ . In this case there are five moments, as specified by

$$\mu'_{mn} = \int R^m \dot{R}^n P \, d\mathbf{x}, \quad (6)$$

where  $m + n = 1$  and  $2$ . An equation for  $P$  follows from a master or population balance equation

$$\frac{dP}{dt} = \frac{\partial P}{\partial t} + \frac{\partial}{\partial R}(P\dot{R}) + \frac{\partial}{\partial \dot{R}}(P\ddot{R}) = 0. \quad (7)$$

Thus, the moment system evolves as

$$\frac{\partial \vec{\boldsymbol{\mu}}'}{\partial t} = \vec{\mathbf{f}}(\vec{\boldsymbol{\mu}}', \mathbf{x}), \quad (8)$$

where  $\vec{\mathbf{f}}$  is over the moments  $\{m, n\}$ :

$$f_{mn} = m\mu'_{m-1, n+1} + n \int \dot{R}(\vec{\mathbf{x}}) R^m \dot{R}^{n-1} P(\vec{\mathbf{x}}, \vec{\boldsymbol{\theta}}) \, d\vec{\mathbf{x}}. \quad (9)$$

In (9),  $\dot{R}$  follows from the bubble dynamics equation and the integration is over the positive half-space in  $R$  and the full space in  $\dot{R}$ . We call this the PDF-based model (or PDF) throughout. (8) is a nonlinear system of integro-differential equations that only represents populations with no third- or higher-order moments. However, a machine-learned forcing term  $\vec{\mathbf{f}}^{\text{ML}}$  appends (8) to represent such moments:

$$\frac{\partial \vec{\boldsymbol{\mu}}'}{\partial t} = \vec{\mathbf{f}}(\vec{\boldsymbol{\mu}}') + \vec{\mathbf{f}}^{\text{ML}}(\vec{\boldsymbol{\mu}}'). \quad (10)$$

A separate single-layer LSTM RNN with 32 time delays comprises  $\vec{\mathbf{f}}^{\text{ML}}$ . Monte Carlo results for  $\vec{\boldsymbol{\mu}}'(t)$  trains the neural network for cases  $p_o/p_\infty = \{0.15, 0.25, \dots, 0.85\}$  trains the neural network. ML denotes this approach hereon. In all cases the second-order accurate Adams–Bashforth method evaluates the time derivative.

### Model bubble dynamics

Non-interacting, isothermal, and surface-tension-neglected gas bubbles present a simple test case

for the method. They follow from a Rayleigh–Plesset-like equation

$$R\ddot{R} + \frac{3}{2}\dot{R}^2 + \frac{4}{Re}\dot{R} = \left(\frac{R_o}{R}\right)^{3\gamma} - \frac{p_\infty}{p_o} \quad (11)$$

where  $\gamma = 1.4$  is the adiabatic compression index,  $p_v$ ,  $p_o$ , and  $p_\infty$  are the vapor, ambient, and liquid far-field pressures,  $Re$  is the Reynolds number, and the pressure ratio  $p_o/p_\infty$  modifies the bubble collapse strength.

### Performance for low-order moments

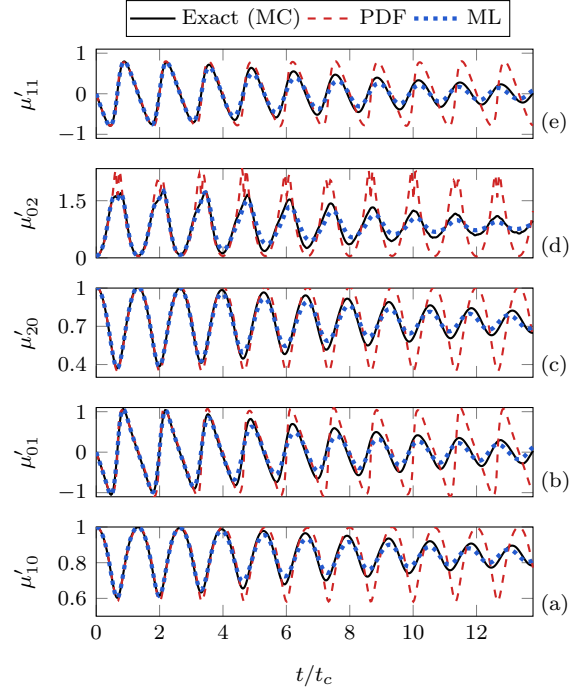


**Figure 6:** Low-order bubble population moments (a)–(e) for  $p_o/p_\infty = 0.3$  using the PDF-based model (PDF), the neural-network-augmented model (ML), and Monte Carlo simulation (exact). The second-order moments are normalized by their  $t = 0$  values and  $t_c$  is the nominal Rayleigh collapse time.

We first evaluate the accuracy of the first- and second-order moments, as determined by the Gaussian distribution function. Figure 6 shows their evolution for a low pressure-ratio  $p_o/p_\infty = 0.3$  case. For both the exact and PDF-based model (PDF) the  $\mu'_{02}$  and  $\mu'_{20}$  moments grow and decay from period-to-period. The covariance moment  $\mu'_{11}$ , and thus correlations between the radii and their velocities, are also significant. The exact moments damp from period-to-period, whereas the moments of the PDF-based model are periodic. Thus, for this low pressure-ratio case the PDF-based model cannot accurately represent the actual statistics. However,

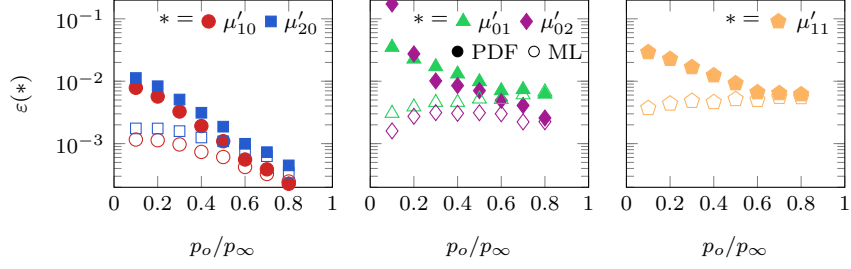


**Figure 7:** Model error  $\varepsilon$  over ten cycles of the mean bubble dynamics for the low-order moments and varying pressure ratio. Both the PDF-based model (PDF) and ML-augmented PDF-based model (ML) are shown.

the machine-learning augmented approach (ML) closely matches the exact result, even for this relatively low pressure-ratio. This includes the relative damping of all moments, which the PDF-based model could not represent.

Figure 7 shows the relative model errors

$$\varepsilon(*) \equiv \frac{\|*_{\text{MC}} - *_{\text{model}}\|_2}{\|*_{\text{MC}}\|_\infty} \quad (12)$$

of the PDF-based model and its augmentation via LSTM RNNs (MC indicates Monte Carlo truth values). For the PDF-based model  $\varepsilon$  increases with decreasing  $p_o/p_\infty$  and bubble velocity moment  $\mu'_{0*}$  errors are largest. For pressure ratios near 1 the dynamics are nearly linear and  $\varepsilon$  is small. The machine learning approach (ML) significantly decreases the model error for all moments for  $p_o/p_\infty \lesssim 0.5$ , while the errors for larger pressure ratios only decrease modestly. For example, for  $p_o/p_\infty = 0.2$  the ML error is only 8% of the PDF error for  $\mu'_{01}$  and 0.9% of it for  $\mu'_{02}$ .

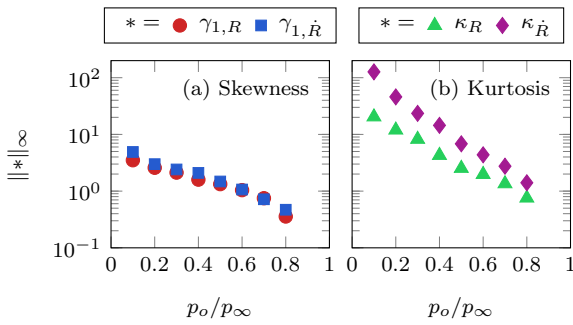


**Figure 8:** (a) Maximum Pearson's moment coefficient of skewness  $\gamma$  and (b) excess kurtosis  $\kappa$  over ten cycles of the mean bubble motion for varying pressure ratio.

The normality of the evolving bubble dynamics determines the validity of the Gaussian PDF used. Figure 8 shows measures of the third- and fourth-order moments that develop during the bubble dynamics. Monte Carlo simulations compute these moments. For  $p_o/p_\infty \rightarrow$

1 the dynamics are nearly linear and  $\gamma_1$  and  $\kappa$  are both small (less than about unity). However, both skewness and kurtosis become large for smaller  $p_o/p_\infty$ :  $\kappa_R = 126.7$  and  $\gamma_{1,R} = 4.9$  for  $p_o/p_\infty = 0.1$ . This skewness results from the slow bubble growth when compared to its rapid collapse. Thus, this PDF-based model cannot represent the low-order moments for small pressure ratios. This explains the increased performance observed for the machine-learning augmented model in figure 7.

### Performance for high-order moments

The ensemble-averaged model requires higher-order functions of the random variables. Following Bryngelson et al. (2019), these are  $\mu'_{3(1-\gamma)0}$ ,  $\mu'_{30}$ ,  $\mu'_{21}$ , and  $\mu'_{32}$ . Since  $P$  is a multivariate Gaussian distribution function, the low-order moments determine the higher-order ones analytically. Adaptive Gaussian quadrature computes the non-integer moment  $\mu'_{3(1-\gamma)0}$  via (6).

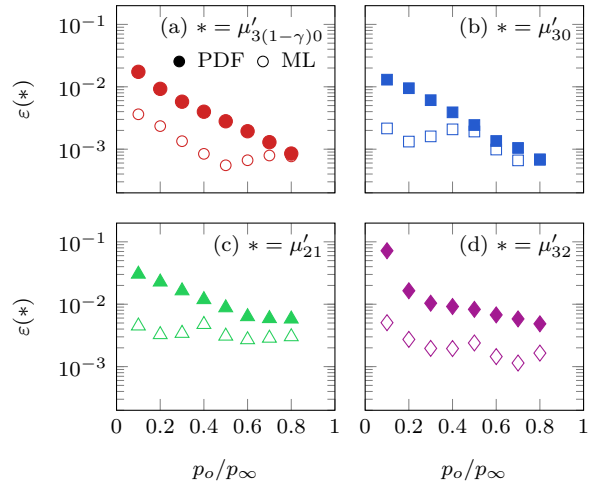


**Figure 9:** Model error  $\varepsilon$  associated with specific distribution moments (a)–(d) for the PDF-based model (PDF) and the ML-augmented PDF-based model augmented with an additional LSTM RNN for these moments (ML).

Figure 9 shows the relative model error of the

ensemble-averaged model moments. Similar to figure 7, the PDF-based model errors grow with decreasing pressure ratio. These errors are large for small  $p_o/p_\infty$ , and the highest-order moment  $\mu'_{32}$  has the largest error. To treat this, we train an additional LSTM neural network with output  $\vec{g}^{\text{ML}}$  as

$$\vec{\mu}'_{\text{ML}} = \vec{\mu}'_{\text{HG}}(\vec{\mu}') + \vec{g}^{\text{ML}}(\vec{\mu}'), \quad (13)$$

where  $\vec{\mu}'_{\text{HG}}$  is the column vector of high-order moments approximated via Gaussian statistics and  $\vec{\mu}'_{\text{ML}}$  are the predictions. The truth-value of the ensemble-averaged moments and  $\vec{\mu}'$  train the neural network  $\vec{g}^{\text{ML}}$ . Figure 9 shows that this approach reduces  $\varepsilon$  from the PDF-based model results for all moments. For example, for  $p_o/p_\infty = 0.1$  the ML error is only 7% of the PDF error for the  $\mu'_{32}$  moment and 20% of it for  $\mu'_{3(1-\gamma)0}$ .

## DISCUSSION AND CONCLUSIONS

We first presented two averaged models: one ensemble-averaging and one volume-averaging. These models can represent dilute bubble flow dynamics, though their implementations and, thus, computational costs differ. The acoustic response of a dilute bubble screen served as a test problem. Results showed that the methods produced the same response, though their computational costs varied, depending on the grid resolution, bubble void fraction, and degree of polydispersity. Ensemble-averaging was cheaper than volume-averaging, except for broadly poly-disperse bubble populations. This resulted from the many bins required to represent the associated bubble dynamics, and thus the poor suitability of the method of classes for such problems.

A moment-based method was formulated to address this issue. It represented and evolved the underlying polydispersity in terms of its statistical moments. This approach was based upon a population balance equation and closed via a Gaussian statistics ansatz for the probability density function. This closure is exact for linear bubble dynamics. Further, it only entails five additional dependent variables: the first- and second-order moments with respect to the Gaussian distribution function. However, for nonlinear Rayleigh–Plesset bubble dynamics the model error can be significant. This error increased with decreasing pressure ratio and thus more violent bubble dynamics. This resulted from the formation of third-, fourth- and possibly higher-order moments. Such moments were not represented by the Gaussian distribution function. Unfortunately, there is no simple approach to represent such high-order moments: higher-order distribution functions often have no unique transformation between the moments and the distribution parameters, and traditional quadrature moment methods become expensive in this regime. Instead, we trained a recurrent neu-

ral network on Monte Carlo truth data to represent such moments, augmenting the dynamics of the low-order moments and improving the evaluation accuracy of the high-order ones. This resulted in significantly smaller model errors for all pressure ratios. For example, for  $p_o/p_\infty = 0.2$  the ML model error was 0.9% of the Gaussian-only moment method for the  $\mu'_{02}$  moment. For the lowest pressure ratio case the error was only 7% of the PDF error for the highest-order ensemble-averaged moment. Future work will implement these models in two-way coupled bubbly flow simulations.

## ACKNOWLEDGEMENTS

This work was supported by the US Office of Naval Research under grant number N0014-17-1-2676.

## REFERENCES

- G. E. Reisman, Y.-C. Wang, C. E. Brennen, Observations of shock waves in cloud cavitation, *J. Fluid Mech.* 355 (1998) 255–283.
- Y. A. Pishchalnikov, O. A. Sapozhnikov, M. R. Bailey, J. C. Williams, R. O. Cleveland, T. Colonius, L. A. Crum, A. P. Evan, J. A. McAteer, Cavitation bubble cluster activity in the breakage of kidney stones by lithotripter shockwaves, *J. Endourol.* 17 (2003) 435–446.
- S. Sharma, K. Mani, V. Arakeri, Cavitation noise studies on marine propellers, *J. Sound Vib.* 138 (1990) 255–283.
- B. Ji, X. Luo, X. Peng, Y. Wu, H. Xu, Numerical analysis of cavitation evolution and excited pressure fluctuation around a propeller in non-uniform wake, *Int. J. Mult. Flow* 43 (2012) 13–21.
- M. Weyler, V. Streeter, P. Larsen, An investigation of the effect of cavitation bubbles on the momentum loss in transient pipe flow, *J. Basic Eng.* 93 (1971) 1–7.
- V. Streeter, Transient cavitating pipe flow, *J. Hydraulic Eng.* 109 (1983) 1407–1423.
- C. E. Brennen, *Cavitation and bubble dynamics*, Oxford University Press, 1995.
- D. Z. Zhang, A. Prosperetti, Ensemble phase-averaged equations for bubbly flows, *Phys. Fluids* 6 (1994).
- A. Biesheuvel, L. van Wijngaarden, Two-phase flow equations for a dilute dispersion of gas bubbles in liquid, *J. Fluid Mech.* 148 (1984) 301–318.
- T. Colonius, R. Hagmeijer, K. Ando, C. E. Brennen, Statistical equilibrium of bubble oscillations in dilute bubbly flows, *Phys. Fluids* 20 (2008).

- M. Vanni, Approximate population balance equations for aggregation breakage processes, *J. Colloid Interface Sci.* 221 (2000) 143–160.
- J. C. Heylmun, B. Kong, A. Passalacqua, R. Fox, A quadrature-based moment method for polydisperse bubbly flows, *Comp. Phys. Comm.* (2019).
- J. Capecelatro, O. Desjardins, An Euler–Lagrange strategy for simulating particle-laden flows, *J. Comp. Phys.* 238 (2013) 1–31.
- Z. Y. Wan, P. Karnakov, P. Koumoutsakos, T. Sapsis, Bubbles in turbulent flows: Data-driven, kinematic models with history terms, *arXiv:1910.02068 Submitted* (2019).
- P. A. Srinivasan, L. Guastoni, H. Azizpour, P. Schlatter, R. Vinuesa, Predictions of turbulent shear flows using deep neural networks, *Phys. Rev. Fluids* 4 (2019) 054603.
- D. Fuster, T. Colonius, Modelling bubble clusters in compressible liquids, *J. Fluid Mech.* 688 (2011) 352–389.
- K. Ando, T. Colonius, C. E. Brennen, Numerical simulation of shock propagation in a polydisperse bubbly liquid, *Int. J. Mult. Flow* 37 (2011) 596–608.
- S. H. Bryngelson, K. Schmidmayer, T. Colonius, A quantitative comparison of phase-averaged models for bubbly, cavitating flows, *Int. J. Mult. Flow* 115 (2019) 137–143.
- K. Maeda, T. Colonius, Eulerian–Lagrangian method for simulation of cloud cavitation, *J. Comp. Phys.* 371 (2018) 994–1017.
- J. B. Keller, M. Miksis, Bubble oscillations of large amplitude, *J. Acoustic. Soc. Am.* 68 (1980).
- K. Ando, Effects of polydispersity in bubbly flows, Ph.D. thesis, California Institute of Technology, 2010.
- S. H. Bryngelson, K. Schmidmayer, V. Coralic, K. Maeda, J. Meng, T. Colonius, MFC: An open-source high-order multi-component, multi-phase, and multi-scale compressible flow solver, 2019. *ArXiv:1907.10512*.
- V. Coralic, T. Colonius, Finite-volume WENO scheme for viscous compressible multicomponent flow problems, *J. Comp. Phys.* 219 (2006) 715–732.
- E. Toro, M. Spruce, W. Speares, Restoration of the contact surface in the HLL-Riemann solver, *Shock waves* 4 (1994) 25–34.
- S. Gottlieb, C.-W. Shu, Total variation diminishing Runge–Kutta schemes, *Math. Comput.* 67 (1998) 73–85.

## DISCUSSION #1

Pablo M. Carrica, Department of Mechanical Engineering, University of Iowa  
Professor

The authors present a very good paper discussing two averaging techniques for cavitating flows, as well as a method to augment a moment-based representation of the size distribution with machine learning.

1. The multigroup method or method of classes can represent any polydisperse size distribution, including bimodal or trimodal shapes, albeit at high cost as the authors point out. The method of moments requires knowing a priori the shape of the size pdf, with considerable cost savings if the result matches the proposed pdf shape. What would be the cost of a method of moments if complex pdf's can be expected from the polydisperse bubbly flow?
2. The improvements shown by the machine learning technique are impressive. Can the authors comment on the potential of using the technique to more complex flows were for instance bubble breakup and coalescence can produce massive changes in size distributions and shapes?
3. Related to 2. and the prognosis to using machine learning for more complex problems, what data would be needed to train the neural networks in a flow situation like sheet to cloud cavitation transition?

## AUTHOR'S REPLY

We thank Professor Carrica for his thoughtful review of our submission.

1. The method used here assumes a pdf shape that remains constant through our simulations. However, this is not a requirement of moment methods generally. Indeed, such a distribution must only be able to be described by a finite set of moments. If the evolving bubble dynamics entail complex distribution shapes, then higher-order moments will be required. For significant pressure ratios, as was shown in Figure 8, such moments (represented by skewness and kurtosis) are significant indeed. Representing these moments explicitly can be expensive for QMOM-based methods, though the ML-based approach here circumvents this via a learned term.
2. The method used here can represent bubble breakup and coalescence via source terms in the population

balance equations. However, it could be computationally expensive to resolve the time-stiff dynamics of the moments that these features entail. Further investigation in this area is required to determine if a ML-based model, perhaps in the spirit of the one used here, can curtail these costs.

3. Direct numerical simulations are sufficient for training a neural network to correct the moments required for bubble-model closure. However, the closure assumptions of the phase-averaged model (e.g., small void fraction) come into question during cloud cavitation transitions. The authors are unaware of theory-based attempts to bridge this chasm, though one is certainly needed before such problems can be solved.

## DISCUSSION #2

Jesse Capecelatro, Department of Mechanical Engineering, University of Michigan  
Assistant Professor

I find that this paper acts as a useful guide for students and scientists in pursuit of developing computationally efficient coarse-grained models for cavitating bubbly flows. It is clear from this work that methods based on ensemble averaging and volume averaging are able to produce similar results, albeit at different cost. This is especially true for polydisperse bubble distributions. To address this, the authors present a novel approach for simulating dilute bubbly flows undergoing cavitation at relatively low computational cost. A machine learning technique is employed, which led to significant improvement of the predictions of high-order moments. While moment methods have demonstrated success in other areas of multiphase flow, it has not been used to simulate cavitating bubble populations. Furthermore, moment closure based on machine learning is new and could have impact outside the context of cavitating bubbly flows.

In this paper, a recurrent neural network was trained on Monte Carlo truth data to inform closure for the high-order moments. If someone wanted to adopt this approach, would they need to repeat this training process, or is there a database where the model closure can be easily adopted? Also, the moment closure problem exists outside of this community. For example, numerical simulations of gas-solid flows sometimes rely on moment methods. A comment on this can be used in that context would be interesting.

## AUTHOR'S REPLY

We thank Professor Capecelatro for his kind comments on our paper. The current model is not in a public database,

instead serving as a demonstration of ML-based closures for moment systems. However, the Monte Carlo simulations it entails are within the computational reach of a single workstation or laptop.

We concur that the moment closure problem is well studied outside of the bubble cavitation, and even bubbly flow literature. For example, the quadrature method of moments (QMOM) can close the moment transport equations. However, QMOM might entail significant computational expense for the complex distributions that form during bubble cavitation. We will address this possibility (and how it complements our machine-learning approach) in future work.